JOURNAL OF COLLOID AND INTERFACE SCIENCE 172, 147–154 (1995)

Measurement of the Drag Coefficient of Spherical Particles Attached to Fluid Interfaces

JORDAN T. PETKOV,[1] NIKOLAI D. DENKOV, KRASSIMIR D. DANOV, ORLIN D. VELEV, RICHARD AUST,* AND FRANZ DURST*

*Laboratory of Thermodynamics and Physico-chemical Hydrodynamics, Faculty of Chemistry, University of Sofia, James Bouchier Avenue 1, 1126 Sofia, Bulgaria; and *LSTM, Technische Fakultät, Friedrich-Alexander-Universität, Cauerstrasse 4, D-91058 Erlangen-Nuremberg, Germany*

Received June 16, 1994; accepted November 2, 1994

The drag coefficient, β, of spherical particles attached to a pure air–water interface is determined. The method is based on the measurement of the particle velocity V, under the action of a well-defined lateral capillary force F. The capillary force is created by controlled deformation of the water surface by means of a Teflon barrier whose vertical position can be precisely adjusted. The magnitude of the force is calculated by means of the theory of capillary interaction between a sphere and a vertical wall (Kralchevsky *et al., J. Colloid Interface Sci.* **167**, 47, 1994). The drag coefficient is calculated from the ratio $\beta = F/V$ at small Reynolds numbers. The dependence of the drag coefficient on the particle size and the three-phase contact angle is determined. For small spheres, which do not create substantial deformation of the fluid interface, β is always smaller than the Stokes coefficient, $\beta_S = 6\pi\eta a$ (η is the water viscosity and a is the particle radius). For large spheres, however, β can be greater than β_S. This higher hydrodynamic resistance can be explained by the presence of a curved meniscus around heavier particles. The measured values of β are compared with theoretical calculations and very good agreement is reached. It is demonstrated that the method is sensitive to the presence of adsorbed surfactants and that it can be used for the determination of the surface viscosity of adsorbed layers.

Key Words: drag coefficient; floating particle; capillary force; three-phase contact angle; surface diffusion.

1. INTRODUCTION

The dynamic behavior of a particle attached to a fluid interface has at least two aspects of interest to the colloid scientist. On the one hand, such a configuration appears in some important technological processes. For instance, particle attachment to the air–liquid interface is an important step in the flotation process (1). On the other hand, the hydrophobic properties of the adsorbed particles (expressed via their three-phase contact angle) are believed to play an important role in the stability of foams and emulsions containing solid or fluid particles (2–4). In coating technology the particles can be either part of the coating material (e.g., latex) or contaminants which cause defects in the final coating (5). As pointed out by Brenner and Leal (6, 7), small spherical particles represent a very convenient model system for the analysis of the equilibrium and the dynamic behavior of adsorbing molecular species (e.g., low-molecular-weight surfactants). In a detailed theoretical study, Brenner and Leal (6, 7) demonstrated how the macroscopic description of the surface adsorption and diffusion can be deduced from a rigorous microscale consideration.

The equilibrium properties of adsorbed particles are relatively well understood. The equilibrium three-phase contact angle of a single solid particle attached to a fluid interface is determined by the minimum of the total interfacial energy and satisfies the Neuman–Young relationship (8). Theoretical expressions are available for the capillary pair interaction energy between adsorbed particles (9–11). Experiments with particles floating in a Langmuir trough were performed (12–14), aimed at determining the three-phase contact angle or other equilibrium properties. In contrast, quantitative studies of the dynamic behavior (diffusion, friction, etc.) of particles attached to a fluid interface are scarce. This results (at least in part) from the theoretical and experimental difficulties which one has to overcome (15). Brenner *et al.* (6, 7, 16–18) considered in general form the problem of determining the diffusion coefficient D and the drag coefficient β of a spherical particle attached to the fluid interface. They showed that the generalized Einstein relation connecting these two coefficients is valid, in this case $D = kT/\beta$ (kT is the thermal energy). For some particular values of the three-phase contact angle, the diffusion and drag coefficients were theoretically calculated (19, 20). In a recent study Danov *et al.* (21) calculated the drag coefficient for a wide range of three-phase contact angles of the particle using the "two vorticities–one velocity" formulation for different values of shear and dilatational surface viscosities. Estimates of the effect of adsorbed surfactants on the dynamics of particle motion were proposed (22, 23). We are aware of only one experimental study where the coefficient of surface diffusion of adsorbed

[1] To whom correspondence should be addressed.

0021-9797/95 $6.00

particles was determined (20). However, because of the small size of the diffusing particles the three-phase contact angle was not determined and controlled in this study. Also, the polydispersity of the sample has not allowed the comparison of these experimental results with theoretical calculations.

Another area where the dynamic properties of adsorbed particles can be important is the process of two-dimensional cluster formation and growth (see Refs. (24–26) and the literature cited therein). In these studies the structure of the aggregates and the kinetic mechanism of their formation are subjects of primary interest.

In the present study we determine the drag coefficient β of relatively large particles (of submillimeter radius) by measuring the particle velocity under the action of a well-defined external force. Compared to previous studies, our method has a number of advantages. First, larger particles allow precise determination of the sphere diameter and the three-phase contact angle. As a result a comparison with available theoretical results (21) is possible without using any adjustable parameters. Second, the measuring method is much faster and, therefore, it is less influenced by disturbing factors like thermal convection (27). Third, the force exerted on the particle is controlled and a set of experiments at different forces are performed. Fourth, as shown below, the method can be applied to systems containing adsorbed surfactant molecules. As a result the rheological properties of the monolayer can be investigated. Once the drag coefficient is known, the diffusion coefficient can be determined by means of the Einstein relation.

It should be noted that this study became possible only after the recent advances in the theoretical and experimental investigation of the lateral capillary forces (28–34). In these papers expressions for the capillary force and the interaction energy between a particle and a vertical wall (or between two particles) are derived and experimentally verified. It is demonstrated that the capillary interactions are quite strong and of a very long range.

This paper is organized as follows. In Section 2 the experimental setup and the materials are described. In Section 3 the data processing procedure is explained. The experimental results are presented and discussed in Section 4. The conclusions are summarized in Section 5.

2. EXPERIMENTAL

2.1. Materials

Most of the measurements were carried out with hydrophobized submillimeter glass spheres. Two different procedures for hydrophobization of the glass beads are used. In one set of experiments the hydrophobization is accomplished by immersion of the precleaned particles for 48 h in a 10^{-2} M solution of cetyltrimethylammonium bromide (CTAB). The surfactant concentration is $\approx$10-fold the critical micelle concentration (CMC). During this period physical adsorption of the cationic surfactant onto the negatively charged glass surface takes place. The three-phase contact angle of the particles prepared by this method is close to 50° (see Section 3.2 for the method of determining the contact angle). In a second set of experiments the compound 1,1,1,3,3,3,hexamethyldisilazane (Sigma, USA) is used as the hydrophobizing agent. This substance provides a chemical bonding between hydrophobic methyl groups and the glass surface as a result of a chemical reaction. For hydrophobization we put some quantity of glass particles on the bottom of a small closed glass beaker. After that we drop a few droplets of the hydrophobizing agent close to the beads inside the beaker and wait for 24 h. The disilazane evaporates from the drops and condenses on the glass particle surfaces. The three-phase contact angles, obtained in this way, are close to 90°. Besides glass beads, measurements were performed with a hydrophobic copper sphere, a product of Stanley Co. (Japan). The sphere has a radius of 0.518 mm and its measured three-phase contact angle was 78°.

The water for the experiments is obtained with a Milli-Q Organex system (Millipore). Before each of the experimental runs the Teflon barrier, glass cell, and glass particles are cleaned by immersion in hot chromic acid for not less than 24 h. This procedure is followed by abundant rinsing with water. Hot chromic acid is also used for cleaning the cuvette and the instrumental glassware.

Sodium dodecyl sulfate (SDS), from Sigma, is used to form a monolayer of surfactant molecules on the air–water interface in one of the experiments. The surfactant is taken from a recently obtained batch quantity and the solutions are prepared 24 h before the experiments. The surfactant concentration is 4×10^{-2} M, which corresponds to fivefold the critical micellar concentration (35).

2.2. Experimental Setup and Procedure

In Fig. 1 the schematics of the experimental equipment used is shown. It presents a modification of the setup described earlier (32), where it was used for the measurement

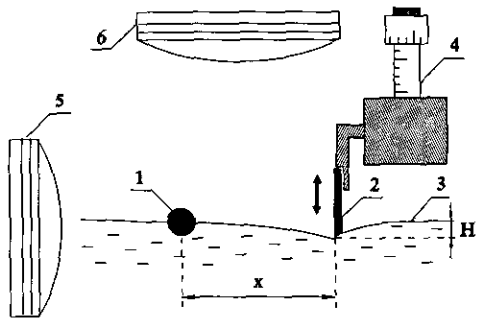

FIG. 1. Experimental setup for determination of the drag coefficient of a particle attached to a fluid interface: (1) spherical particle, (2) movable Teflon barrier, (3) fluid interface, (4) micrometric screw, (5) horizontal long-focus microscope, (6) vertical long-focus microscope.

of the lateral capillary image force between spherical particles and a vertical wall. The equipment contains horizontal and vertical microscopes (Carl Zeiss-Jena, Germany). Through the vertical microscope the motion of the particle can be observed and recorded by using a CCD camera and video recorder (SLV-R5, Sony). The horizontal microscope allows the measurement of the particle dimensions in order to calculate the three-phase contact angle at the particle surface (see Section 3.2 below).

Before each experimental run, the aqueous phase is poured inside the vessel and its surface is cleaned from impurities by suction of the liquid via a pipette connected to a vacuum pump. After cleaning, the hydrophobized glass particle is put on the air–water surface by using a glass capillary holder. The Teflon barrier (see Fig. 1) is connected to a micrometric table which allows measurement of the depth of barrier movement downward. In order to achieve sufficient accuracy we repeat the initial adjustment of the zero level (where the barrier touches the water surface, $H = 0$, see Fig. 1) 20–30 times and take the average number from the micrometer scale. Then the barrier is moved downward until a certain depth, H, is achieved. This leads to a deformation of the water surface and results in a lateral capillary force exerted on the particle (31), which brings about particle movement toward the wall of the barrier. The video recording of the moving particle is then processed frame by frame using a Videoplan 2 computer from Zeiss (Germany), and the distance between the particle and the wall is measured as a function of time. When the particle reaches the wall the Teflon barrier is lifted by using the micrometric screw. Due to the change of the meniscus slope at the Teflon surface, the particle is repelled and again moves away from the wall. Then the Teflon barrier can be moved downward again and the measurement can be performed at a different depth H. When experiments with SDS are carried out, the system is left to relax for not less than 2 min before each measurement in order to accomplish equilibrium between the surfactant monolayer and the bulk solution.

In order to reduce evaporation during the experiment, the equipment is placed in an isolating transparent box saturated with water vapor.

3. DATA PROCESSING

3.1. Capillary Force and Drag Coefficient

The physical origin of the capillary interaction between a floating particle and a wall lies in the fact that the wall perturbs the interfacial deformation created by the particle (31). The range of the capillary interaction can be characterized by the so-called capillary length, q^{-1},

$$q^2 = \Delta\rho g/\gamma, \quad \Delta\rho = \rho_{\mathrm{I}} - \rho_{\mathrm{II}}, \qquad [3.1]$$

where γ is the interfacial tension, ρ_{I} and ρ_{II} are the mass densities of the two fluid phases, and g is the gravity acceleration. Thus for a water–air interface ($\Delta\rho = 1000$ kg/m^3, $\gamma = 72$ mN/m) one has $q^{-1} = 2.7$ mm.

According to the theory developed by Kralchevsky *et al.* (31), when the particle–wall separation is large compared to the particle diameter, the capillary force exerted on the particle is given by the following asymptotic expression:

$$F = -\pi\gamma[-2qQ_2^2K_1(2qx) + 2Q_2qHe^{-qx} + q(r_2qHe^{-qx})^2]. \qquad [3.2]$$

Here, $Q_2 = r_2\sin\Psi_2$ is the so-called "capillary charge" of the floating particle, r_2 is the radius of the three-phase contact line at the particle surface, and Ψ_2 is the meniscus slope angle at the particle three-phase contact line (see Fig. 2). $K_1(2qx)$ is a modified Bessel function of the first order. H is the depth of immersion of the Teflon barrier with respect to the plane $z = 0$, and x is the distance between the particle center and the wall surface. In our study the capillary charge of the particle was calculated through the expression (11, 31)

$$Q_2 = \frac{1}{2}q^2\left[\left(R_2 - \frac{b_2}{3}\right)b_2^2 - \frac{4}{3}D_2R_2^3 - r_2^2h_2\right], \qquad [3.3]$$

where R_2 is the particle radius and

$$D_2 = \frac{(\rho_2 - \rho_{\mathrm{II}})}{(\rho_{\mathrm{I}} - \rho_{\mathrm{II}})}, \qquad [3.4]$$

where ρ_2 is the particle density. In Eq. [3.3], b_2 is the depth of particle immersion inside the lower phase (Fig. 2). It was directly measured as explained in Section 3.2 (the dependence of b_2 on the particle–wall separation is a higher-order effect for the particles studied). The quantity h_2 is the mean elevation of the particle contact line with respect to the horizontal surface $z = 0$. In our calculations we used the asymptotic expression (31)

$$h_2 = h_{2\infty} + H\exp(-qx) - Q_2K_0(2qx), \qquad [3.5]$$

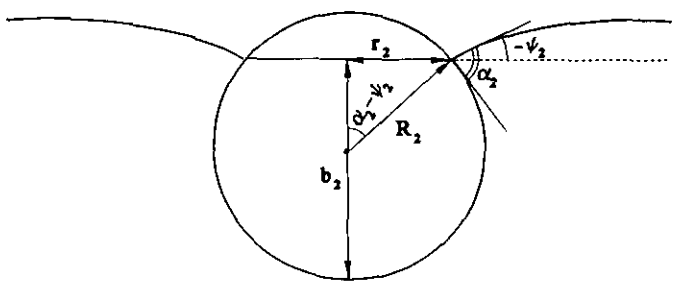

FIG. 2. Sketch of a spherical particle attached to a fluid interface. R_2 is the particle radius and α_2 is the three-phase contact angle.

where $h_{2\infty}$ corresponds to a single particle situated far away from the wall. $h_{2\infty}$ was calculated by using Derjaguin's formula (36),

$$h_{2\infty} = Q_{2\infty} \ln\left(\frac{2}{\gamma_e q r_2}\right); \qquad [3.6]$$

$\gamma_e = 1.781071\cdots$ in Eq. [3.6] is the constant of Euler–Masceroni and

$$Q_{2\infty} = \frac{1}{6} q^2 R_2^3 (2 - 4 D_2 + 3 \cos\alpha_2 - \cos^3\alpha_2) \qquad [3.7]$$

is the limiting value of Q_2 for $x \to \infty$ (see Ref. (11)).

In order to obtain the trajectory of the particle, it is necessary to solve the equation of motion,

$$m\ddot{x} = F - \beta\dot{x}, \qquad [3.8]$$

where β is the particle drag coefficient and F is given by Eq. [3.2]. The drag force is expressed as

$$F_d = -\beta\dot{x} = -f_d\beta_s\dot{x}, \qquad [3.9]$$

where

$$\beta_s = 6\pi\eta R_2 \qquad [3.10]$$

is the Stokes drag coefficient for a sphere immersed in an unbounded fluid and f_d denotes the dimensionless drag coefficient for a particle floating on the interface. In final form,

$$\ddot{x} = \frac{F}{m} - f_d\frac{\beta_s}{m}\dot{x}. \qquad [3.11]$$

This nonlinear differential equation can be solved numerically by transforming it into a system of two differential equations of the first order,

$$\begin{cases} \dot{V} = F/m - f_d\dfrac{\beta_s}{m} V. \\ \dot{x} = V. \end{cases} \qquad [3.12]$$

The numerical solution of these two differential equations, at fixed boundary conditions, gives us the motion law of the particle, $x(t)$ and $V(t)$, as well as the value of f_d considered as an adjustable parameter.

In the present study the drag coefficient is determined by comparing the measured dependence of the particle–wall separation, x, vs time, t, with the theoretical function calculated by means of numerical integration of the particle motion equation. As a merit function in the minimization procedure we used the so-called "random middle deviation of squares" (RMDS),

$$\text{RMDS} = \frac{1}{N}\sum_{k=1}^{N}\left(1 - \frac{x_{th,k}}{x_{exp,k}}\right)^2, \qquad [3.13]$$

where N is the number of experimental points taken into account, and $x_{th,k}$ and $x_{exp,k}$ are the theoretical predictions and the experimental results at a given time.

3.2. *Determination of the Particle Three-Phase Contact Angle*

The quantities R_2, b_2, and r_2 are directly measured by using the horizontal microscope (Figs. 1 and 2). Then one can use either the values of R_2 and b_2 or the values of R_2 and r_2 to calculate α_2 and the meniscus slope angle Ψ_2 by using a simple iterative procedure described in Section 3 of Ref. (32).

4. RESULTS AND DISCUSSION

Experimental data measured as explained above are shown in Figs. 3–5. Figure 3 shows the measured trajectories $x(t)$ of a glass sphere of radius $R_2 = 0.229$ mm and a three-phase contact angle of $\alpha_2 = 48.7°$. The different symbols correspond to different values of the immersion depth H. The larger the H, the greater the capillary force F at a given separation x (the two upper curves in the figure intersect because the initial moments at $t = 0$ correspond to different initial values $x(t = 0)$). The value of the dimensionless drag coefficient determined from the minimization of RMDS (Eq. [3.13]) is $f_d = 0.68 \pm 0.02$. It is seen from the figure that the theoretical curves and the experimental points agree very well except

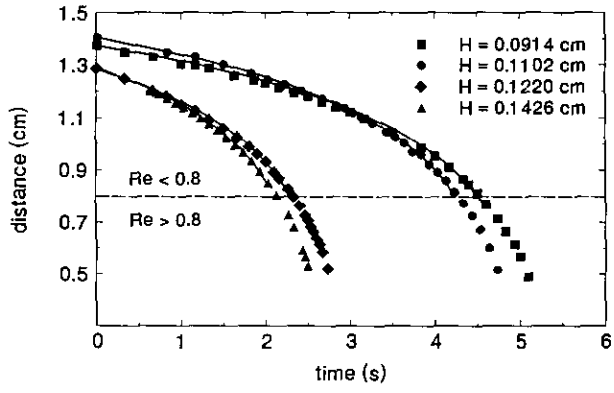

FIG. 3. Trajectories of a spherical glass particle of radius $R_2 = 0.229$ mm and three-phase contact angle $\alpha_2 = 48.7°$. The symbols denote experimental points and the solid lines are calculated by means of the numerical procedure described in Section 3.1 with the dimensionless drag coefficient $f_d = 0.68 \pm 0.02$. The different curves correspond to different magnitudes of the water surface deformation, H.

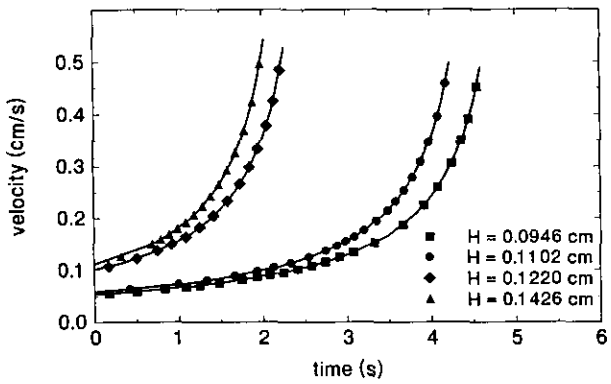

FIG. 4. Velocity of a spherical glass particle (the same as in Fig. 3) as measured experimentally (the symbols) and calculated (the solid curves) from the numerical procedure with $f_d = 0.68 \pm 0.02$.

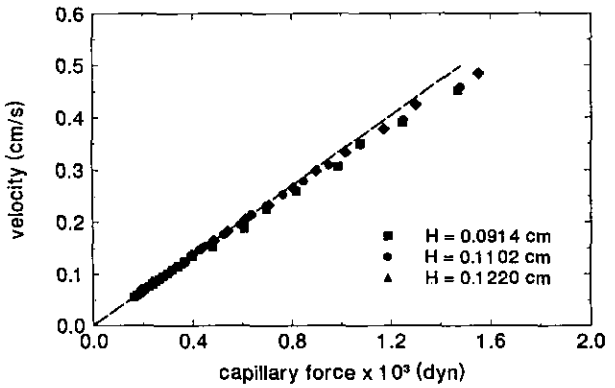

FIG. 5. Velocity of a glass particle as a function of the capillary force calculated by means of Eq. [3.2]. The slope of the straight line corresponds to drag coefficient $f_d = 0.68$ without inertial effects.

for the region of the smallest separations ($x < 8$ mm). The poorer agreement in this region is most probably due to the following reasons: (i) the particle velocity (and the corresponding Reynolds number) becomes so high that inertial hydrodynamic effects become important; (ii) the capillary force at separations $qx \sim 1$ may not be accurately calculated from Eq. [3.2], which is an asymptotic expression valid at $(qx)^2 > 1$; and (iii) the presence of the Teflon barrier may influence the hydrodynamic flow around the particle and thus may change the value of f_d, due to hydrodynamic interaction between the particle and the wall. That is why in the minimization procedure we use only the points above the horizontal dashed line in Fig. 3 corresponding to $x > 8$ mm, i.e., Re < 0.8, where the asymptotic expression for the capillary force is justified. In this region the perturbation of the hydrodynamic flow around the particle due to the Teflon barrier can be neglected because the distance between the bead and the barrier is about 40 times the particle radius (it is well known from hydrodynamics that this interaction obeys an inverse proportional law with respect to the distance $\propto 1/x$).

In Fig. 4 the measured and calculated particle velocities are compared. The experimental points are in excellent agreement with the theoretical curves for all experimental runs. The measured particle velocity is plotted in Fig. 5 as a function of the capillary force calculated by using Eq. [3.2]. The dashed straight line in the figure corresponds to the simple proportional law of particle motion (negligible inertial effects),

$$F = -\beta V = -f_d \beta_s V,$$

with $f_d = 0.68$. At larger separations the points of all experimental runs lie on the straight line because the particle acceleration term ($m\ddot{x}$) on the left-hand side of Eq. [3.8] is negligible compared with the capillary and drag forces. However, at small separations (larger capillary force) one observes a deviation of the experimental points from the straight line, due to a contribution of the acceleration term in the force balance (Eq. [3.8]). The points in that region are very well described theoretically when one accounts for the acceleration term, as in Eq. [3.12]—see Figs. 3 and 4.

In a similar way, we processed the experimental data for glass spheres of different three-phase contact angles and the final results are summarized in Table 1. It is seen from Table 1 that the dimensionless drag coefficient f_d of the glass beads on pure water decreases with the increase of the particle three-phase contact angle and is always smaller than unity. The theoretical analysis performed by Brenner and Leal (6, 7) shows that the dimensionless drag coefficient of a particle attached to a planar fluid interface is a function only of the ratio of the viscosities of the two fluids and of the three-phase contact angle. Therefore, for pure water–air interfaces and light particles (which slightly deform the interface) f_d does not depend on the particle size. The function $f_d(\alpha_2)$ is numerically calculated in Ref. (21) and is plotted in Fig. 6 together with our experimental results. As seen from the figure, the agreement between theory and experiment is very good. One should note that no adjustable parameters are used in this comparison.

The experiments with the heavier copper particle, however, showed that f_d can be larger than unity (i.e., that the dimen-

TABLE 1
Measured Drag Coefficients of Glass and Copper Particles with Different Three-Phase Contact Angles

System type	α_2 (°)	R_2 (mm)	f_d	SD
1. Glass bead	48.7	0.229	0.68	±0.02
2. Glass bead	53.0	0.231	0.66	±0.03
3. Glass bead	82.0	0.222	0.54	±0.05
4. Copper bead	78.0	0.518	1.77	±0.05
5. Glass bead + surfactant	52.0	0.216	1.60	—

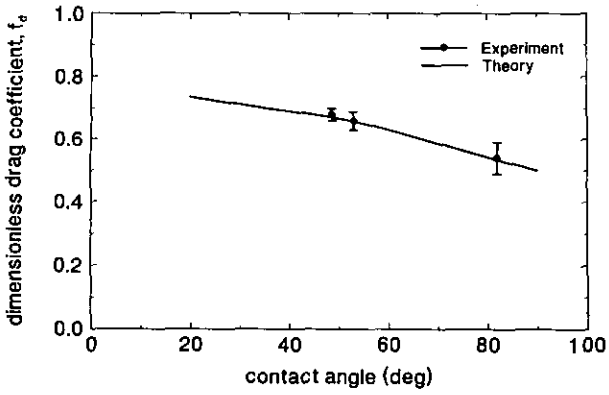

FIG. 6. Comparison of the experimental results (the circles) for the dimensionless drag coefficient with the theoretical calculations from Ref. (21).

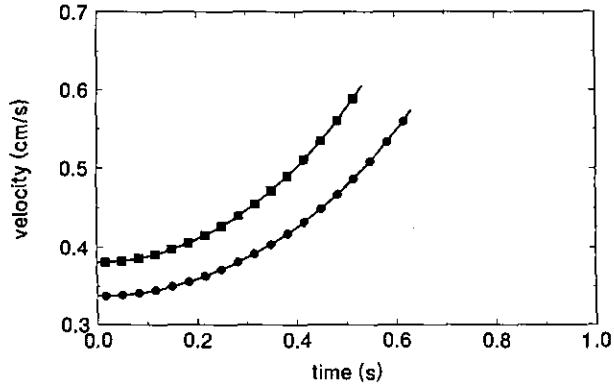

FIG. 8. Comparison of the experimentally measured (the symbols) and the theoretically calculated (the solid curves) velocities of the copper bead for the data shown in Fig. 7.

sional drag coefficient β can be larger than the Stokes coefficient). As an illustration, in Fig. 7 two measured trajectories of the copper sphere (R_2 = 0.518 mm and α_2 = 78°), corresponding to two different values of H, are plotted. The solid curves are calculated by using the procedure from Section 3.1, and the values f_d = 1.75 for the upper curve and f_d = 1.83 for the lower curve are determined. As explained in Ref. (38), this high drag coefficient can be considered as a result of the increased hydrodynamic resistance in the curved meniscus region formed around the heavier particle. The main reason for the increased hydrodynamic resistance, resulting in a higher surface drag coefficient of the particle, is the movement of the curved meniscus around the particle together with the particle itself. This leads to a bulk motion of the fluid, and the dissipation takes place not only at the immersed surface of the particle, but in the whole region below the curved meniscus. For that reason, the surface drag coefficient becomes almost three times bigger than the expected value at the same three-phase contact angle (when only the friction of the particle surface beneath the water–air interface is considered). The lower the deformation of the meniscus, the lower the difference between the measured dimensionless drag coefficient and its theoretically predicted value. The limiting case is the situation where there is no meniscus deformation around the particle. In this case the measured values coincide very well with the theoretical ones (see Fig. 6). The measured and calculated velocities for the same experimental runs are compared in Fig. 8. Again, a very good agreement is observed.

Finally, we present results for the drag coefficient of a particle moving along the air–water interface when a monolayer of adsorbed surfactant molecules is present. The experimental data were measured with a disilazane hydrophobized glass bead of radius R_2 = 0.216 mm, whose contact angle α_2 was determined to be 52°. The results are presented in Figs. 9 and 10 and in the last row of Table 1. The trajectory

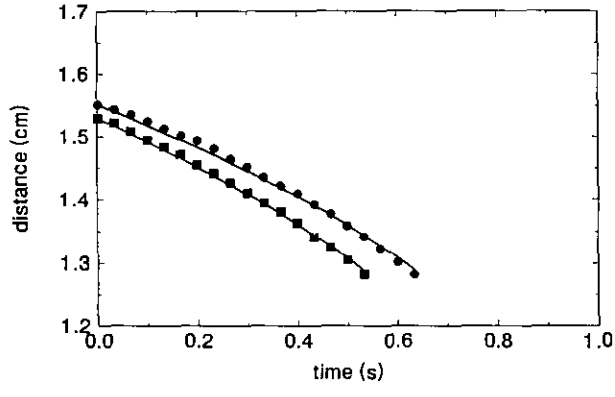

FIG. 7. Trajectory of a copper particle with radius R_2 = 0.5178 mm and three-phase contact angle α_2 = 78° at two different depths of immersion of the Teflon barrier: H = 0.942 mm and H = 1.031 mm. The solid lines are calculated with dimensionless drag coefficient f_d = 1.75 (the upper curve) and f_d = 1.83 (the lower curve).

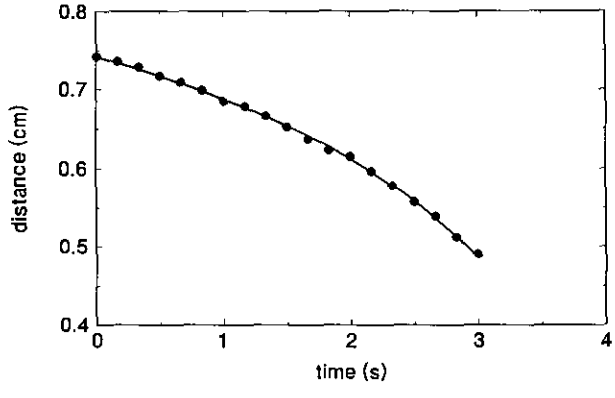

FIG. 9. Trajectory of a spherical glass particle of radius R_2 = 0.216 mm and three-phase contact angle α_2 = 52.0° in the presence of 4×10^{-2} M sodium dodecyl sulfate. The symbols denote experimental points and the solid line is calculated by means of the numerical procedure described in Section 3.1, with dimensionless drag coefficient f_d = 1.60.

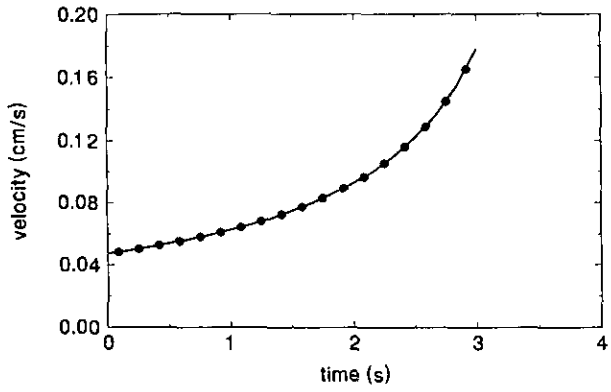

FIG. 10. Velocity of a spherical glass particle in the presence of surfactant (compare with Fig. 9) as measured experimentally (the symbols) and calculated (the solid curves) from the numerical procedure with $f_d = 1.60$.

of the particle, plotted in Fig. 9, is described fairly well by the above theoretical expressions (Eqs. [3.11] and [3.12]) with an adjustable parameter $f_d = 1.60$. The good agreement between theory and experiment is also demonstrated in Fig. 10, where the data are plotted as particle velocity vs time. It is seen that the presence of a surfactant monolayer increases the dimensionless drag coefficient f_d from 0.663 (theoretical for pure liquids; see Fig. 6) to 1.60. This considerable difference can be interpreted as a result of the surface viscosity of the SDS adsorption layer (37). Our data suggest that the developed method is very sensitive to the presence of surfactant molecules adsorbed on a surface.

5. CONCLUSIONS

The main new results of this study can be summarized as follows:

(i) A relatively simple and precise method for the determination of the drag coefficient β of a spherical particle attached to a liquid interface has been developed. The accuracy and reproducibility of the data correspond to a relative error in β smaller than 5%.

(ii) Measurements of the drag coefficient of submillimeter glass spheres on a pure water surface at different three-phase contact angles were performed. The measurements show that for these particles β is smaller than the Stokes coefficient $\beta_s = 6\pi\eta R_2$ and decreases with the three-phase contact angle α_2. For such light particles the dimensionless drag coefficient $f_d = \beta/\beta_s$ is a function of α_2 and does not depend on the particle size. The comparison of the experimental results for $f_d(\alpha_2)$ with available theoretical calculations shows a very good agreement (see Fig. 6) without using any adjustable parameter.

(iii) The experiments with heavier copper spheres show that β can be larger than the Stokes coefficient β_s. This nontrivial result can be explained by the higher hydrodynamic resistance in the curved meniscus formed around the heavy particles.

(iv) The presence of an adsorbed monolayer of surfactant molecules increases appreciably the surface drag coefficient of the particles. This fact suggests the attractive possibility of investigation of the rheological properties of the monolayer.

The proposed method can be applied without substantial modifications to the following important systems: a water surface covered with a nonsoluble or soluble surfactant (including proteins) and the interface between two liquids (e.g., water and oil). From the drag coefficient one can calculate the surface diffusion coefficient by means of the Einstein relation.

ACKNOWLEDGMENTS

The authors thank Professor Peter A. Kralchevsky and Dr. Hans Raszillier for their most helpful discussions. This research was supported financially by Volkswagen-Stiftung. The authors gratefully acknowledge this support of their collaborative research.

REFERENCES

1. Schulze, H. J., "Physico-chemical Elementary Processes in Flotation." Elsevier, Amsterdam, 1984.
2. Aveyard, A. R., Cooper, P., Fletcher, P. D. I., and Rutherford, C. E., *Langmuir* **9**, 604 (1993).
3. Denkov, N. D., Kralchevsky, P. A., Ivanov, I. B., and Wasan, D. T., *J. Colloid Interface Sci.* **150**, 589 (1992).
4. Tambe, D. E., and Sharma, M. M., *J. Colloid Interface Sci.* **157**, 244 (1993).
5. Chevalier, Y., Pichot, C., Graillat, C., Joanicot, M., Wong, K., Maquet, J., Lindner, P., and Cabane, B., *Colloid Polym. Sci.* **270**, 806 (1992).
6. Brenner, H., and Leal, L. G., *J. Colloid Interface Sci.* **65**, 191 (1978).
7. Brenner, H., and Leal, L. G., *J. Colloid Interface Sci.* **88**, 136 (1982).
8. Tadros, Th. V., and Vincent, B., *in* "Encyclopedia of Emulsion Technology" (P. Becher, Ed.), Vol. 1, p. 129. Dekker, New York, 1983.
9. Nicolson, M. M., *Proc. Cambridge Philos. Soc.* **45**, 288 (1949).
10. Chan, D. Y. C., Henry, J. D., Jr., and White, L. R., *J. Colloid Interface Sci.* **79**, 410 (1981).
11. Paunov, V. N., Kralchevsky, P. A., Denkov, N. D., and Nagayama, K., *J. Colloid Interface Sci.* **157**, 100 (1993).
12. Aveyard, R., Binks, B. P., Fletcher, P. D. I., and Rutherford, C. E., *J. Chem. Soc. Faraday Trans.*, in press.
13. Armstrong, A. J., Mockler, R. C., and O'Sullivan, W. J., *J. Phys. Condens. Matter* **1**, 1707 (1989).
14. Clint, J. H., and Taylor, S. E., *Colloids Surf.* **65**, 61 (1992); Clint, J., and Quirke, N., *Colloids Surf. A: Phys.-Chem. Eng. Aspects* **78**, 277 (1993).
15. Kim, S., and Karrila, S., "Microhydrodynamics: Principles and Selected Applications." Butterworth–Heinemann, Boston, 1991.
16. Goldman, A. J., Cox, R. G., and Brenner, H., *Chem. Eng. Sci.* **22**, 637, 653 (1967).
17. Schneider, Y. C., O'Neill, M. E., and Brenner, H., *Mathematika* **20**, 175 (1973).
18. Majumdar, S. R., O'Neill, M. E., and Brenner, H., *Mathematika* **21**, 147 (1974).
19. Wakiya, S., *Colloid Eng. Res. Rep.* **6** (March 30, 1957).
20. Radoev, B., Nedjalkov, M., and Djakovich, V., *Langmuir* **8**, 2962 (1992).
21. Danov, K. D., Aust, R., Durst, F., and Lange, U., *J. Colloid Interface Sci.*, in press.

22. Mileva, E., and Nikolov, L., *J. Colloid Interface Sci.* **161,** 63 (1993).
23. Dimitrov, K., Radoev, B., and Avramov, M., *Langmuir* **9,** 1414 (1993).
24. Meakin, P., *Faraday Discuss. Chem. Soc.* **83,** 113 (1987).
25. Jullien, R., Botet, R., and Mors, P. M., *Faraday Discuss. Chem. Soc.* **83,** 125 (1987).
26. Hórvölgyi, Z., Medveczky, G., and Zrinyi, M., *Colloids Surf.* **60,** 79 (1991).
27. Mysels, K. J., *Langmuir* **8,** 3191 (1992).
28. Kralchevsky, P. A., Paunov, V. N., Ivanov, I. B., and Nagayama, K., *J. Colloid Interface Sci.* **151,** 79 (1992).
29. Kralchevsky, P. A., Paunov, V. N., Denkov, N. D., Ivanov, I. B., and Nagayama, K., *J. Colloid Interface Sci.* **155,** 420 (1993).
30. Paunov, V. N., Kralchevsky, P. A., Denkov, N. D., Ivanov, I. B., and Nagayama, K., *Colloids Surf.* **67,** 119 (1992).
31. Kralchevsky, P. A., Paunov, V. N., Denkov, N. D., and Nagayama, K., *J. Colloid Interface Sci.* **167,** 47 (1994).
32. Velev, O. D., Denkov, N. D., Paunov, V. N., Kralchevsky, P. A., and Nagayama, K., *J. Colloid Interface Sci.* **167,** 66 (1994).
33. Kralchevsky, P. A., Denkov, N. D., Paunov, V. N., Velev, O. D., Ivanov, I. B., Yoshimura, H., and Nagayama, K., *J. Phys. Condens. Matter* **6,** 1 (1994).
34. Velev, O. D., Denkov, N. D., Paunov, V. N., Kralchevsky, P. A., and Nagayama, K., *Langmuir* **9,** 3702 (1993).
35. Lindman, B., and Wennerström, H., *Top. Curr. Chem.* **87,** 1 (1980).
36. Derjaguin, B. V., *Dokl. Akad. Nauk USSR* **51,** 517 (1946).
37. Davies, J. T., and Rideal, R. K., "Interfacial Phenomena." Academic Press, London, 1963.
38. Danov, K. D., Durst, F., and Raszillier, H., submitted for publication.